Kovove Mater. 50 2012 301–307
DOI: 10.4149/km_2012_5_301

Interaction between phase transformation and compression sintering in a TiAl-based intermetallic alloy

M. Charpentier[1], D. Daloz[1,3], A. Hazotte[2,3]*

[1]*Institut Jean Lamour (IJL), CNRS/Université de Lorraine, Ecole des Mines de Nancy, Parc de Saurupt, 54042 NANCY Cedex, France*
[2]*Laboratoire d'Etude des Microstructure et de Mécanique des Matériaux (LEM3), CNRS/Université de Lorraine, Île du Saulcy, 57045 METZ Cedex 1, France*
[3]*DAMAS, Laboratory of Excellence on Design of Alloy Metals for low-mass Structures, Université de Lorraine, France*

Received 11 January 2012, received in revised form 13 April 2012, accepted 13 April 2012

Abstract

The metastable structure of a Ti-48Al-2Cr-2Nb atomised powder is analysed by X-ray diffraction (XRD) and scanning electron microscopy (SEM), revealing that it mostly contains the α disordered phase, with traces of γ and β/B2 phases. Then, the evolution of the alloy towards its stable (γ + α_2) structure during continuous heating is studied by differential thermal analysis (DTA), differential scanning calorimetry (DSC) and XRD of heat treated powders. Transformation takes place in a narrow temperature domain, ranging between 620 °C and 700 °C. It is characterised by a transformation enthalpy of about 2200 J mol^{-1}. Uniaxial compression during continuous heating reveals a transient consolidation of the powder in this transformation range, with a relative magnitude of about 1.9 % for a compression stress of 100 MPa. It is proposed that this phenomenon could be due to phase transformation plasticity.

K e y w o r d s: titanium aluminides, based on TiAl, phase transformation, plastic deformation mechanisms, powder metallurgy, including consolidation, microstructure

1. Introduction

Although casting still appears attractive for TiAl-based intermetallic alloys, their high reactivity in the liquid state as well as the segregation inherited from solidification lead to severe restriction for using this process. This gives way to the opportunity to develop other routes. Among them, the powder metallurgy seems promising, either through conventional rolling or hipping of atomised powder [1] or through more recently developed techniques based on spark plasma sintering of atomised and/or crushed materials [2]. While neither medium nor long-range segregation is noticeable with these PM routes, the main challenge is to ensure full and reproductive densification, if possible in short times and/or at low temperatures. For that reason, most part of the current research in this field is devoted to the optimisation of processing parameters. Only a few works focused on the material structure history during the process, i.e. the way the non-equilibrium structure of gas-atomised Ti-Al powders evolves during the process, up the final microstructure of the consolidated alloy.

In this paper, we focus on the first step of consolidation of a Ti-48Al-2Cr-2Nb alloy (GE alloy) through non-isothermal uniaxial compression. We firstly characterise the initial metastable structure of the powder, then analyse its evolution toward equilibrium during continuous heating. Finally, we determine the effect of this structure evolution on the material behaviour during consolidation.

2. Experimental procedure

The alloy under study was the so-called 'General Electric' (GE) alloy, which chemical composition is centred around 48at.%Ti-48%Al-2%Cr-2%Nb. The atomised powder was supplied by Crucible Materials Corporation and produced by inert gas atomisation.

*Corresponding author: tel: +33 3 87 31 56 44; e-mail address: alain.hazotte@univ-lorraine.fr

Table 1. Chemical composition of the powder under study

Element	Ti	Al	Cr	Nb	0
at.%	48.32 ± 0.97	47.62 ± 0.95	2.00 ± 0.04	1.92 ± 0.04	0.14 ± 0.01

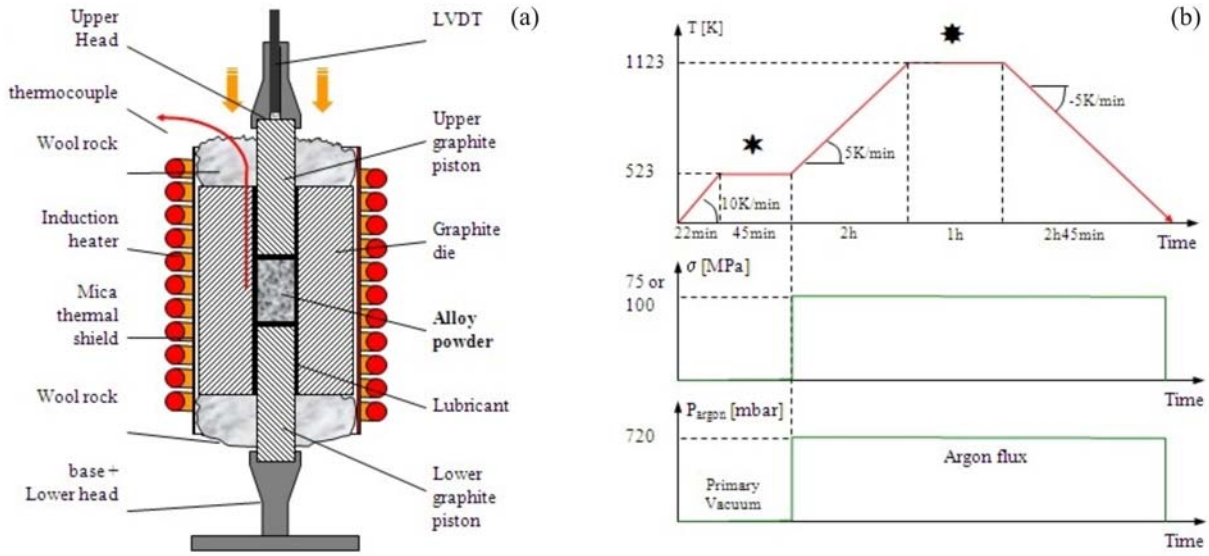

Fig. 1. a) Schematisation of the apparatus used for unidirectional compression sintering, b) temperature, stress and gas flux cycles performed.

Its actual composition was measured through inductively coupled plasma (ICP) spectrometry and is reported in Table 1. Particle size distribution was measured through a Coulter LS 50 laser granulometer. Particle diameters range up to 200 μm, with median and mode at 86.2 μm and 116.3 μm, respectively.

The phases present in GE powders were determined through X-ray diffraction (XRD) in $\theta/2\theta$ mode, using a Siemens Kristalloflex 760 diffractometer, with a D500 goniometer and a Co anticathode ($\lambda[K_{\alpha 1}] = 0.178897$ nm). The microstructures were observed through scanning electron microscopy in both secondary electron (SEM-SE) and back scattered electron (SEM-BSE) modes, using a PHILIPS FEG XL30S equipment.

The evolution encountered by the atomised powder during simple heating was studied by differential thermal analysis (DTA) and differential scanning calorimetry (DSC), using Setsys 1600 and DSC 111 Setaram equipments, respectively. Continuous heating/cooling were performed from 293 K to 1373 K at different rates under argon flux. Pure alumina was chosen as reference sample. Heat treatments in furnace were also performed on powders wrapped in a tantalum foil, then sealed into quartz bulbs under primary vacuum. These treatments consisted in heating at 5 K min^{-1} at different temperatures for 5 min, then rapid cooling in air. The treated powders were used for XRD characterisation of the phases present at different temperatures.

Sintering under unidirectional compression was performed on cylinders of GE powder, using an original equipment developed in our laboratory (IJL) and schematised in Fig. 1a. Figure 1b illustrates the applied thermal and mechanical cycles, which were performed under argon flux. A continuous heating at 5 K min^{-1} was applied from 250 °C up to 850 °C. The maximum sintering temperature was maintained for one hour. A constant macroscopic compression stress of 100 MPa was applied during the whole cycle. Several samples were treated. Their final density was measured by quantitative analysis of optical micrographs, which gave an average volume fraction of about 80 %.

3. Results and discussion

3.1. Powder characterisation

Figure 2 shows four almost spherical powder particles with different sizes observed in SEM-SE mode. CR and SR values reported on the micrographs are the cooling and solidification rates, respectively.

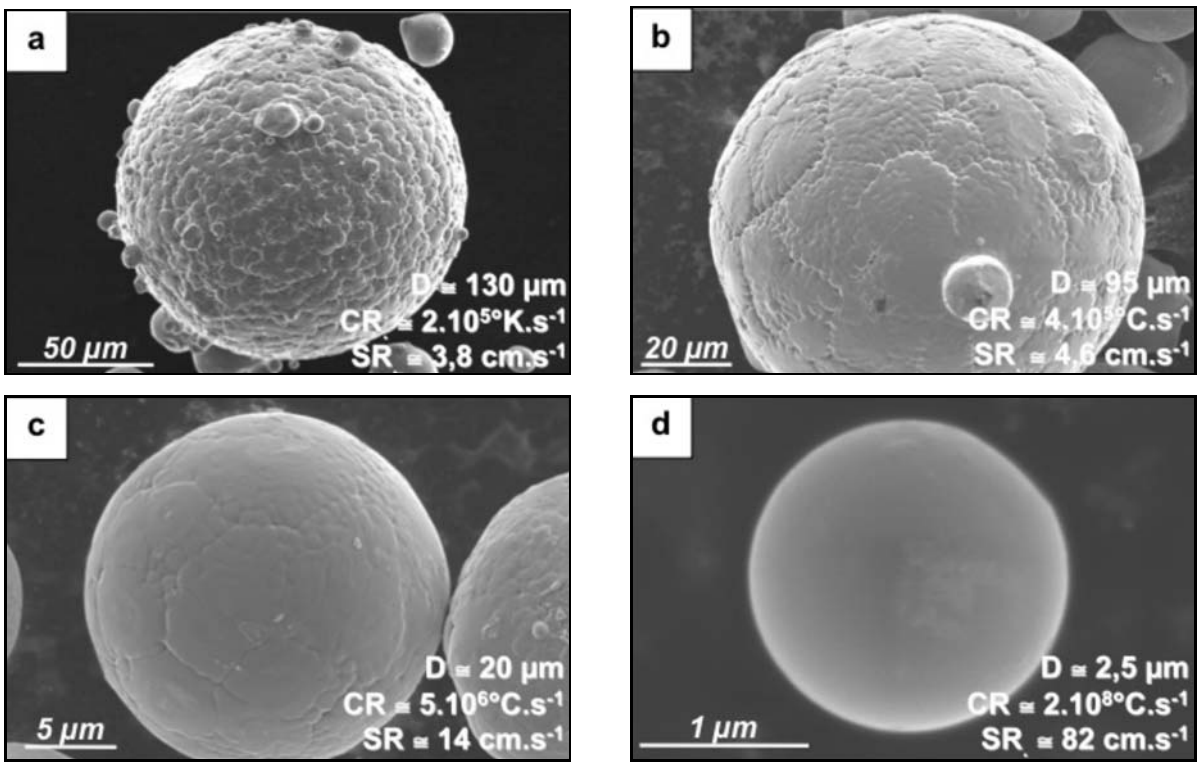

Fig. 2a–d. Different shapes of powder surfaces as a function of the particle diameter D.

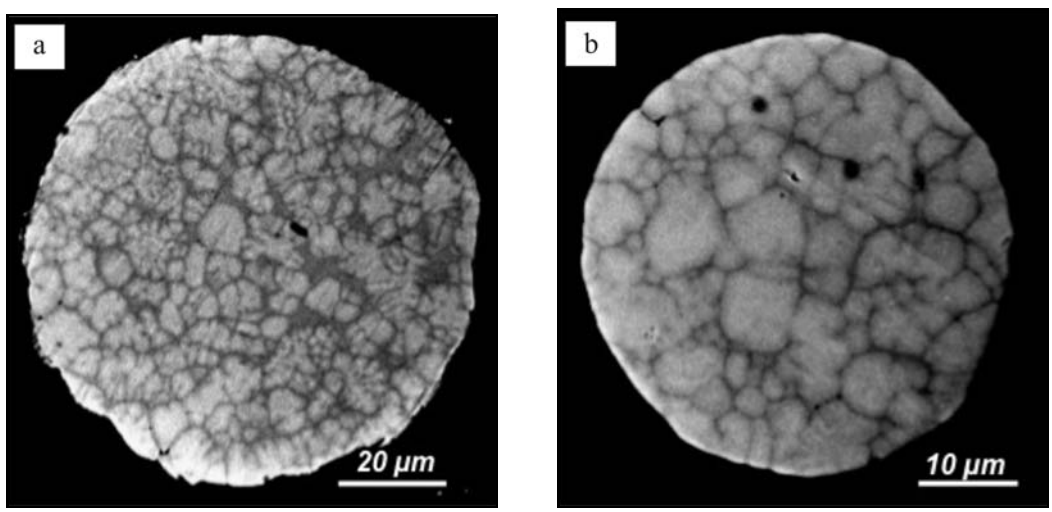

Fig. 3a,b. SEM-BSE images from sectioned powder particles, showing the chemical segregation associated with solidification.

They were roughly estimated using the empirical formulae proposed in [3, 4]:

$$\mathrm{CR} = 11.56 \times \frac{1 + 17.95\sqrt{D}}{D^2},$$

$$\mathrm{SR} = 0.016 \times \frac{1 + 17.95\sqrt{D}}{D},$$

where D is the diameter of the powder grain. Particle surface shows characteristic undulations, which are directly related to the solidification dendritic structure, as illustrated by the SEM-BSE images reported in Fig. 3. It can be noted the microstructure evolution as a function of the solidification rate: from dendritic (Fig. 2a,b) to mix cellular/dendritic (Figs. 2c, 3a) to cellular (Fig. 3b) and plane front for the smaller particle (Fig. 2d).

A typical $\theta/2\theta$ powder diffractogram recorded on initial GE atomised powder is reported on Fig. 4. It shows that the as-atomised powder mostly contains

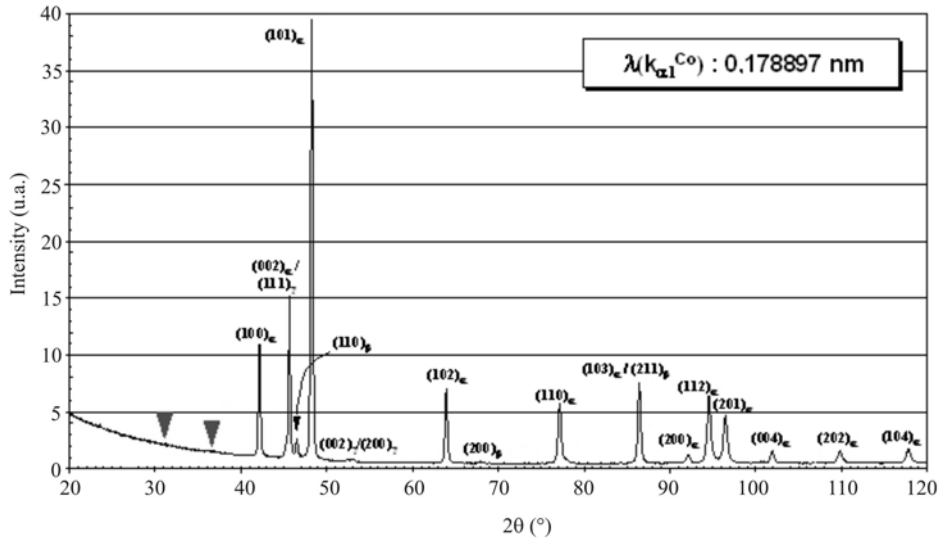

Fig. 4. $\theta/2\theta$ diffractogram of initial GE powder, with indication of the characteristic peaks; triangles point the 2θ positions of the more intense substructure peaks of ordered α_2 phase.

a hexagonal phase. Due to the absence of substructure peaks associated with DO_{19} ordered α_2 phase, this hexagonal phase was identified to be the A3 disordered α phase. Note that a diffractogram was also performed on a bulk super-alpha2 alloy [5, 6] to verify that, in that case, the more intense substructure peaks of DO_{19} structure can effectively be detected with our experimental configuration. Some peaks associated with $L1_0$ γ phase and with A2 β (or ordered B2) phase were also detected in the powder XRD pattern. Table 2 reports the phase volume fractions and lattice parameters extracted from the diffractogram using the Rietveld fitting method. Lattice parameters are in agreement with values previously measured on GE powder by Fuchs and Hayden [7] or on Ti-50Al--2Nb powders by Shih et al. [8].

Several works already pointed out that a large amount of out-of-equilibrium hexagonal phase could be retained in atomised Ti-Al powders, due to the high cooling rate involved in the process [7–14]. When discussed, the nature of this phase was proposed to be either α [7–9] or/and α_2 [10–13]. Actually, the type of retained phase is probably strongly dependent on the atomisation conditions, especially on the cooling/solidification rate. Consequently, in a given powder batch, it could also depend on the size of powder particles. Therefore, it is even possible that a low fraction of ordered phase can be present in the largest particles of our powder, i.e. the ones expected to solidify with the lowest rate. The presence of γ and β/B2 phases is also reported in previous works, although with a very large range of measured amounts. Some authors observed that β/B2 phase is mostly found in dendrite cores, whereas γ rather concentrates in the interdendritic zones [9, 14]. With regard to the low amount of these phases in our powders, we did not focus on this question in the present work.

Table 2. Volume fractions and lattice parameters of the different phases detected in the initial GE powder, as measured through X-ray diffractometry

Phase	Amount (%)	a (nm)	c (nm)
α	91.4	0.2867	0.4603
γ	5.3	0.4007	0.4049
β/B2	3.4	0.3199	

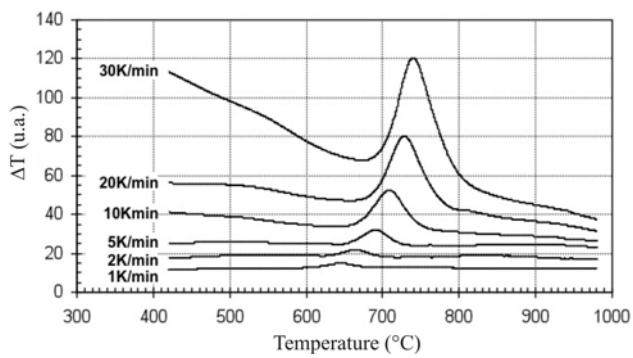

Fig. 5. Evolution of DTA curves during heating at different rates, starting from as-atomised powders.

3.2. Powder evolution toward equilibrium during heating

Figure 5 shows DTA curves recorded during heating at different rates ranging from 1 K min^{-1} to 30 K min^{-1}. Exothermal peaks are clearly detected on

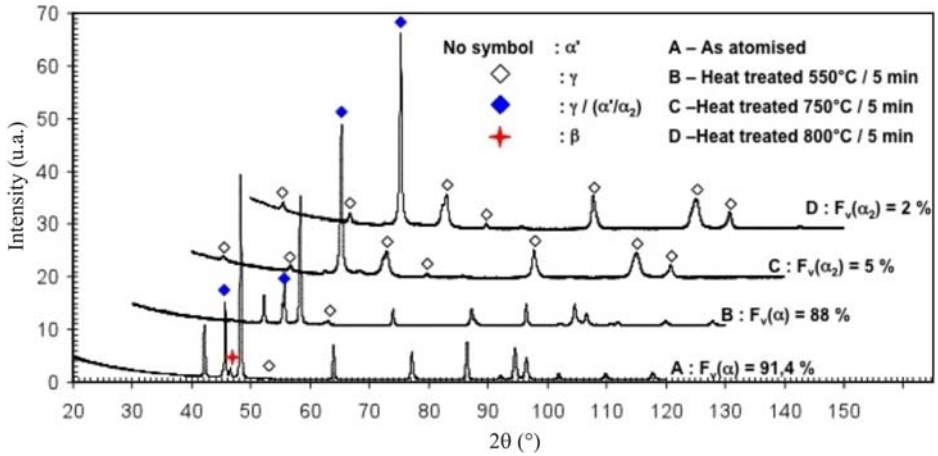

Fig. 6. Comparison of diffractograms recorded for the as-atomised GE powder (the same as in Fig. 3) and for powders heat treated for 5 min at 550 °C, 750 °C and 800 °C.

Table 3. Volume fractions and lattice parameters of the different phases detected in GE powders heat treated for 5 min at different temperatures (heating rate 5 °C min^{-1}; final cooling in air)

Heat treatment	phase	amount (%)	a (nm)	c (nm)
5 min 550 °C	γ	12	0.4004	0.4044
	α	88	0.2861	0.4603
5 min 750 °C	γ	95	0.401	0.405
	α_2	5	0.5702	0.4618
5 min 800 °C	γ	98	0.4008	0.4052
	α_2	2	0.5696	0.4622

every curve. They are observed neither during subsequent cooling nor during second heating. Thus, we conclude that these peaks mark the phase transformation from $(\alpha + \gamma + \beta/\mathrm{B2})$ to $(\alpha_2 + \gamma)$, the latter being the equilibrium state below 1373 K for this alloy. However, since no double regime could be detected in the transformation range, we were not able to discriminate between α to α_2 and α/α_2 to γ transformations from neither DTA nor DSC curves. As proposed by McQuay [15], we linearly interpolated the temperature of maximum thermal shift, as well as the temperatures of starting and finishing transformation down to zero heating rate. This allows estimating the critical temperature for structure destabilisation at about 660 °C and the transformation range between 620 °C and 700 °C. These values are in agreement with previous studies. Schaefer and Janowski [10] reported a critical temperature of 705 °C for a Ti-45Al alloy, while Jabbar et al. [14] measured a transformation range between 650 °C and 850 °C in the case of a Ti-47Al-1Re-1W-0.2Si alloy heated at 100 °C min^{-1}.

By integration over temperature of similar transformation peaks obtained by DSC, we obtained an estimation of $(\alpha \rightarrow \alpha_2 + \gamma)$ transformation enthalpy equal to 57 J g^{-1}, i.e. 2210 J mol^{-1} if molar mass is taken equal to 38.8 g mol^{-1}. This value is slightly higher than the one measured by Schaefer and Janowski [10], which was equal to 41 J g^{-1} (1580 J mol^{-1}). The difference may be explained by the fact that the initial structure of [10] was mostly constituted of α_2 phase, i.e. was closer to equilibrium. However, it is worthwhile to note that both values are almost three times lower than those expected from thermodynamic calculations [16].

X-ray diffraction on heat treated samples confirmed the transformation from the initial structure mostly constituted of α phase (Fig. 4 and Table 2) toward a structure constituted of γ and α_2 phases*. This is illustrated in Fig. 6, which compares diffractograms recorded for the initial structure and after heat treatments for 5 min at 550 °C, 750 °C and 800 °C (heating rate 5 °C min^{-1}). Table 3 also collects the phase volume fractions and lattice parameters measured after these treatments. It can be verified that most

* Note that due to the very small amount of α/α_2 phase after heat treatments, substructure peaks can no more be detected on diffractograms. Only thermodynamic consideration allows us to assume that the hexagonal phase retained at low temperature is α_2 phase.

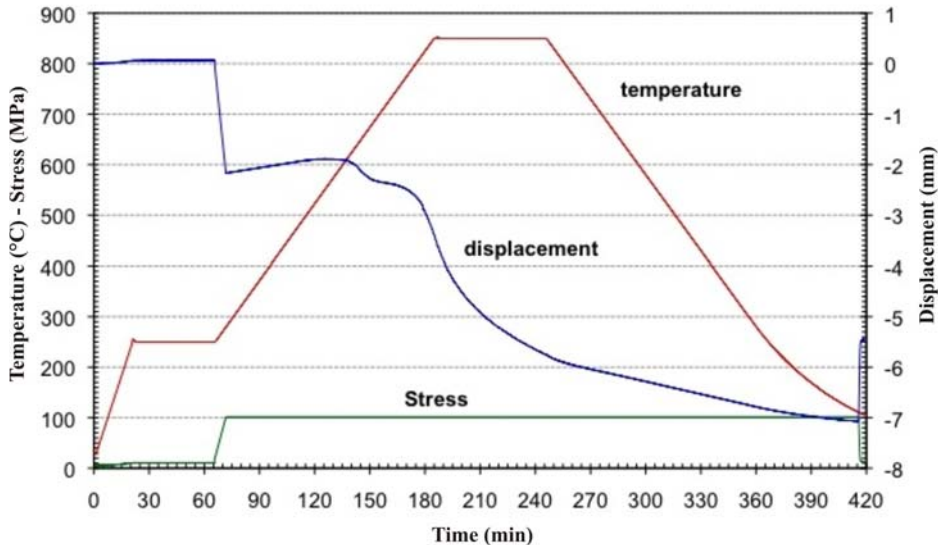

Fig. 7. Evolutions of temperature, applied stress and piston displacement recorded during one consolidation cycle.

part of the $\alpha \rightarrow \alpha_2 + \gamma$ transformation takes place between 550 ℃ and 750 ℃. It can also be noted that the β/B2 phase present in the as-atomised powder is no more detected after treatment at 550 ℃, suggesting that it should dissolve at the benefit of γ phase during heating. No significant difference in lattice parameters was detected after the heat treatments.

3.3. Compression sintering

Figure 7 reports the displacement of the mobile compression die recorded during a whole sintering cycle under 100 MPa. In addition to the successive expected evolutions due to stress application, dilation during heating, sintering under stress at higher temperature, contraction during cooling and finally stress release, the curve shows a singularity ranging from 600 ℃ to 700 ℃ during heating, which is associated with an apparent transient densification of the powder. This singularity was observed for all experiments performed in the present work. Considering that the measured displacement is only related to powder compaction (high stiffness of the compression device), the density increase associated with this singularity – equal to the relative linear contraction – is estimated to be about 1.9 %. This assumption is still reinforced by the fact that the final density estimated by the same way is about 84 %, i.e. rather close to the one measured by image analysis.

It is evident that the transient contraction detected between 600 ℃ and 700 ℃ during heating should be related with the $\alpha \rightarrow (\gamma + \alpha_2)$ phase transformation pointed out in §3.2. The transition from α to γ under applied stress is actually expected to induce a variation in sample dimension due to three different effects: a) difference of density between both phases, b) difference of stiffness and c) phase transformation plasticity (PTP), i.e. extra-plasticity due to the development of internal stresses during phase transformation [17–20]. Although γ phase is actually denser than α [21], dilatometric characterisation of the transformation of 100 % of α into almost 100 % of γ during cooling showed that the associated contraction extrapolated at 600 ℃ was less than 0.3 % [22]. We did not find any precise data relative to the Young's modulus of α and γ phases at 600 ℃, but it is unlikely that their difference could be at the origin of a contraction of 2 %. Consequently, we propose that the contraction should be related to phase transformation plasticity. This well-known phenomenon could occur in two different ways: a) plastic deformation of the weaker phase under the combined actions of applied stress and local internal stress due to the difference of density between phases (the so-called 'Greenwood-Johnson mechanism' [19]) or b) selection of particular γ crystallographic variants, which orientations favour the deformation imposed by local stresses state ('Magee mechanism' [20]). The former mechanism can be activated in any type of transformation. The latter requires that parent and new phases present strict orientation relationships between each other, therefore allowing selection of favourable orientations and habit planes during transformation. This is actually the case for $\alpha \rightarrow \gamma$ transformation, in which both phases are related by the so-called 'Blackburn's orientation relationship' expressed by: $\{111\}_\gamma$ // $(0002)_\alpha$ and $<1\bar{1}0]_\gamma$ // $<11\bar{2}0>_\alpha$ [22–26]. The determination of which mechanism is predominant – if any – would require deeper microstructure investigation. This study is in progress. It is particularly tricky since deformation of sintered powders is complex and often heterogeneous, due to large stress gradients encountered

at the particle scale [14]. Moreover, a sintering process stopped at 700 °C, i.e. just after the phase transformation, does not allow to recover compact samples required for precise observations through microscopy techniques.

4. Summary

This experimental work focused on the structure evolution of metastable powders of a Ti-48Al-2Cr-2Nb alloy during unidirectional compression sintering. It has been shown that:

– The initial microstructure of as-atomised powder grains was mainly composed of α phase with low fractions of γ and β phases.

– During continuous heating, this highly metastable structure goes back to the equilibrium $(\gamma + \alpha_2)$ one; the critical temperature for structure destabilisation was found to range between 620 °C and 700 °C; associated transformation enthalpy was estimated about 57 J g^{-1}, i.e. 2210 J mol^{-1}.

– Under a 100 MPa unidirectional compression stress, a transient densification of about 1.9 % relative magnitude is observed during the structure evolution.

– This extra-densification could be associated with the phenomenon of phase transformation plasticity.

Acknowledgements

The present work was carried out as a part of the French Research Program CPR Intermétalliques Base Titane. The authors are indebted to Ing. P. Brunet who developed the sintering equipment, and to Dr. X. Devaux for granulometry measurements.

References

[1] Bystrzanowski, S., Bartels, A., Clemens, H., Gerling, R., Schimansky, F. P., Dehm, G.: Intermetallics, *13*, 2005, p. 515. doi:10.1016/j.intermet.2004.09.001

[2] Orru, R., Licheri, R., Mario Locci, A., Cincotti, A., Cao, G.: Mater. Sci. Eng., *R63*, 2009, p. 127.

[3] Cai, X. Z., Eylon, D.: In: Proc. of the 8th World Conference on Titanium – Titanium '95: Science and Technology. Eds.: Blenkinsop, P. A., Evans, W. J., Flower, H. M. London, The Institute of Materials 1996, p. 455.

[4] Cai, X. Z., Eylon, D.: In: Proc. of the 8th World Conference on Titanium – Titanium '95: Science and Technology. Eds.: Blenkinsop, P. A., Evans, W. J., Flower, H. M. London, The Institute of Materials 1996, p. 467.

[5] Blackburn, M. J., Smith, M. P.: Titanium Alloys of the Ti3Al Type. UK Patent GB 20606938, 1984.

[6] Kerry, S., Winstone, M. R.: Mater. Sci. Eng., *A 192/193*, 1995, p. 856. doi:10.1016/0921-5093(95)03336-X

[7] Fuchs, G. E., Hayden, S. Z.: Mater. Sci. Eng., *A 152*, 1992, p. 277. doi:10.1016/0921-5093(92)90079-G

[8] Shih, D. S., Scarr, G. K., Chesnutt, J. C.: In: High Temperature Ordered Intermetallic Alloys III. Eds.: Liu, C. T., Taub, A. I., Stoloff, N. S., Koch, C.C. MRS 1988, p. 167.

[9] McCullough, C., Valencia, J. J., Levi, C. G., Mehrabian, R.: Mater. Sci. Eng., *A 214*, 1990, p. 83. doi:10.1016/0921-5093(90)90337-3

[10] Schaefer, R. J., Janowski, G. M.: Acta Metal. Mater., *40*, 1992, p. 1645. doi:10.1016/0956-7151(92)90107-P

[11] Zhao, L., Beddoes, J., Wallace, W.: In: High Temperature Ordered Intermetallic Alloys V. Eds.: Baker, I., Darolia, R., Whittenberger, J. D., Yoo, M. H. MRS 1992, p. 921.

[12] Gouma, P. I., Saunders, N., Loretto, M. H.: Mater. Sci. Technol., *12*, 1996, p. 823. doi:10.1179/026708396790122279

[13] Habel, U., Yolton, C. F., Moll, J. H.: In: Gamma Titanium Aluminides 1999. Eds.: Kim, Y.-W., Dimiduk, D. M., Loretto, M. H. TMS 1999, p. 301.

[14] Jabbar, H., Monchoux, J. P., Thomas, M. et al.: Intermetallics, *18*, 2010, p. 2312. doi:10.1016/j.intermet.2010.07.024

[15] McQuay, P. A.: Mater. Sci. Eng., *185*, 1994, p. 55. doi:10.1016/0921-5093(94)90927-X

[16] Charpentier, M.: [PhD Thesis Report]. Nancy, INPL 2003.

[17] Gautier, E., Simon, A., Beck, G.: Acta Metall., *35*, 1987, p. 1367. doi:10.1016/0001-6160(87)90019-8

[18] Dunand, D. C., Bedell, C. M.: Acta Mater., *44*, 1996, p. 1063.

[19] Greenwood, G. W., Johnson, R. H.: Proc. Roy. Soc., *283A*, 1964, p. 403.

[20] Magee, C. L.: Transformation Kinetics, Microplasticity and Ageing of Martensite in Fe-3l-Ni. [PhD Thesis Report]. Pittsburgh, Carnegie Mellon University 1966.

[21] Zhang, D., Dehm, G., Clemens, H.: Scripta Mater., *42*, 2000, p. 1065. doi:10.1016/S1359-6462(00)00341-9

[22] Charpentier, M., Hazotte, A., Daloz, D.: Mater. Sci. Eng., *A 491*, 2008, p. 321. doi:10.1016/j.msea.2008.02.009

[23] Blackburn, M. J.: In: The Science, Technology and Applications of Titanium. Eds.: Jaffee, R. I., Promisel, N. E. Oxford, Pergamon Press 1970, p. 633.

[24] Denquin, A., Naka, S.: Acta Mater., *44*, 1996, p. 343. doi:10.1016/1359-6454(95)00167-4

[25] Zghal, S., Naka, S., Couret, A.: Acta Mater., *45*, 1997, p. 3005. doi:10.1016/S1359-6454(96)00398-9

[26] Dey, S., Hazotte, A., Bouzy, E.: Intermetallics, *17*, 2009, p. 1052. doi:10.1016/j.intermet.2009.05.013